Creation of a needle of longitudinally polarized light in vacuum using binary optics

HAIFENG WANG[1]*, **LUPING SHI**[1], **BORIS LUK'YANCHUK**[1], **COLIN SHEPPARD**[3] **AND CHONG TOW CHONG**[1,2]

[1]Data Storage Institute (DSI), Agency for Science, Technology and Research, DSI Building, 5 Engineering Drive 1, 117608 Singapore
[2]Department of Electrical & Computer Engineering, National University of Singapore, 4 Engineering Drive 3, 117576 Singapore
[3]Division of Bioengineering, National University of Singapore, 7 Engineering Drive 1, 117574 Singapore
*e-mail: wang_haifeng@dsi.a-star.edu.sg

Recently many ideas have been proposed for the use of a longitudinal field for particle acceleration, fluorescent imaging, second-harmonic generation and Raman spectroscopy. A few methods to enhance the longitudinal field component have been suggested, but all have insufficient optical efficiency and non-uniform axial field strength. Here we report a new method that permits the combination of very unusual properties of light in the focal region, permitting the creation of a 'pure' longitudinal light beam with subdiffraction beam size (0.43λ). This beam is non-diffracting; that is, it propagates without divergence over a long distance (of about 4λ) in free space. This is achieved by focusing a radially polarized Bessel–Gaussian beam with a combination of a binary-phase optical element and a high-numerical-aperture lens. This binary optics works as a special polarization filter enhancing the longitudinal component.

Over the past decade great success has been achieved in the creation of radially polarized light[1–3]. However, the creation of longitudinally polarized light has been a big challenge until now. A plane electromagnetic wave is purely transversal. Thus, for many years it was assumed that it was impossible to create longitudinally polarized light in free space. Since then it has been shown that any beam of finite diameter has a longitudinal field component, even in free space[4,5]. A strong longitudinal component appears at the focal region of a tightly focused laser beam[5–8]. It also arises with the focusing of radially polarized light[1–3,9–13]. Besides being of academic interest, this longitudinal field has many attractive applications, for example, in particle acceleration[5,9,10,14], fluorescent imaging[15], second-harmonic generation[16–18] and Raman spectroscopy[19]. It can permit the achievement of higher resolution in z-polarized confocal fluorescence microscopy[20] and scattering scanning near-field optical microscopy[21].

The longitudinal field can be suppressed or enhanced by amplitude, polarization and phase modulation of the incident beam[22]. For example, a longitudinal field can be completely suppressed in an azimuthally polarized beam[1,23]. Several methods for enhancing the longitudinal field component have been suggested[2,9,22,24,25]; however, all have insufficient optical efficiency (at the level of a few per cent), and the strength of the longitudinal component decreases rapidly away from the beam waist. Conversion efficiency is a critical characteristic for real applications, such as the use of radially and azimuthally polarized laser radiation for material processing[26], put into practice soon after the development of effective methods for radial and azimuthal beam polarization.

RESULTS

The conversion efficiency is not the only parameter that requires improvement. In an ideal situation we want to have a longitudinally polarized beam in free space with subdiffraction size that is uniform along the optical axis (a so-called non-diffracting beam). Although it seems to be rather questionable that this problem can be solved (to the best of our knowledge from the published papers), we want to demonstrate that it is possible to combine all of these contradictory requirements using a hybrid lens (a combination of a binary-phase optical element and a high-numerical-aperture lens) to focus a radially polarized Bessel–Gaussian beam[27,28]. Calculations show that it is possible to achieve a high efficiency of conversion for a beam that is almost longitudinally polarized along the optical axis. The full–width at half-maximum (FWHM) of the beam is 0.43λ and it propagates without divergence for a distance of $\sim 4\lambda$.

DIRECT FOCUSING OF THE RADIALLY POLARIZED BESSEL–GAUSSIAN BEAM

First we review some effects of the non-diffracting beam problem. This idea comes from the exact solution of the Maxwell equations in terms of cylindrical waves. The zero-order Bessel beam mode, with amplitude proportional to $J_0(k_r r)\exp(-ik_z z)$, where k_r and k_z are wave vectors in the r and z directions, respectively, and J_0 is the zero-order Bessel function, propagates in free space without diffraction[6,9–11,24,29]. This kind of beam exists in infinite free space and is polarized perpendicular to the propagation direction in the paraxial approximation. Although the zero-order Bessel function is not square integrable and an infinite power is therefore necessary to create a non-diffracting beam, some nearly
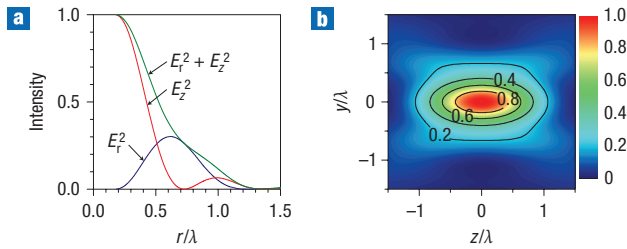
Figure 1 Electric energy density in the focal region of a NA = 0.95 lens illuminated with a radially polarized Bessel–Gaussian beam. a, Radial component E_r^2, longitudinal component E_z^2 and the total electric energy density $E_r^2 + E_z^2$ on the focal plane. **b**, Contour plot of the total electric energy density distribution on the $y-z$ cross-section.

Figure 2 Schematic of the set-up. Radially polarized beam, phase-modulation optical element and focusing lens.

non-diffracting beams (for example, Bessel–Gaussian, Laguerre–Gaussian, Hermite–Gaussian[27,30–32]) with finite power can be realized and can propagate over a long range without significant divergence. Following the general theory of focusing of polarized beams[4] one can write the following equations for the electric fields near the focus $z = 0$ for illumination of the high-aperture lens with the waist of a radially polarized Bessel–Gaussian beam[9,11,28]:

$$E_r(r,z) = A \int_0^\alpha \cos^{1/2}\theta \sin(2\theta)\ell(\theta)J_1(kr\sin\theta)e^{ikz\cos\theta}\mathrm{d}\theta \quad (1)$$

and

$$E_z(r,z) = 2iA \int_0^\alpha \cos^{1/2}\theta \sin^2\theta\,\ell(\theta)J_0(kr\sin\theta)\,e^{ikz\cos\theta}\mathrm{d}\theta. \quad (2)$$

Here we have adopted notations similar to ref. 28: $\alpha = \arcsin(\mathrm{NA}/n)$, where NA is the numerical aperture and $n = 1$ is the index of refraction of free space, $J_0(x)$ and $J_1(x)$ denote Bessel functions, and the function $\ell(\theta)$ describes the amplitude distribution of the Bessel–Gaussian beam, which is given by[28]

$$\ell(\theta) = \exp\left[-\beta^2\left(\frac{\sin\theta}{\sin\alpha}\right)^2\right]J_1\left(2\gamma\frac{\sin\theta}{\sin\alpha}\right), \quad (3)$$

where β and γ are parameters that we take as unity in our configuration. Illumination with a Laguerre–Gaussian beam is very similar. The NA of the focusing lens is 0.95 ($\alpha \approx 71.8°$). The corresponding field distribution is shown in Fig. 1.

The first zero point in the distribution of radial electric density is $r_0 = 1.07\lambda$ in Fig. 1a,b. Then the integral $\Phi_z = 2\pi \int_0^{r_0} |E_z(r,0)|^2 r\,\mathrm{d}r$ from the longitudinal component characterizes the longitudinal energy within the directional lobe in the focal plane. A similar integral Φ_r from the radial field component characterizes the radial energy. The beam quality is characterized by $\eta = \Phi_z/(\Phi_z + \Phi_r)$, which is 0.45 in Fig. 1a. Thus, the parasitic radial field yields about 55% of the total electric energy. This is quite a general effect, which one can also see with other generalized Bessel–Gaussian beams[30]. This radial field also leads to a broadening of the beam. As a result, the beam size has a full-width at half-maximum (FWHM) as large as 0.68λ, which is larger than the diffraction limit for this focusing lens
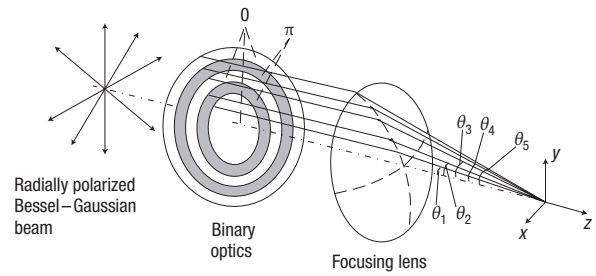
$\lambda/(2\mathrm{NA}) = 0.526\lambda$. However, the beam size contributed by the longitudinal field component is only 0.49λ. Although it is possible to enhance the longitudinal component of the beam in the focal plane with higher NA, the depth of focus also decreases with higher NA.

EFFECTS OF BINARY OPTICS

It is desirable to enhance the longitudinal field component and also achieve long depth of focus. We show that it is possible to generate this non-diffracting longitudinal beam by applying an additional binary optical element on the lens aperture. As is shown in Fig. 2, formally this corresponds to replacing the function $\ell(\theta)$ in equations (1) and (2) by the function $\ell(\theta)T(\theta)$, where the transmission function $T(\theta) = \exp[i\varphi(\theta)]$. If the elements are set with $\varphi(\theta) = 0$ or $\varphi(\theta) = \pi$ for different ranges of angle θ this corresponds to a binary mask[33,34]. We use a five-belt optical element with

$$T(\theta) = \begin{cases} 1, & \text{for } 0 \le \theta < \theta_1,\ \theta_2 \le \theta < \theta_3,\ \theta_4 \le \theta < \alpha, \\ -1, & \text{for } \theta_1 \le \theta < \theta_2,\ \theta_3 \le \theta < \theta_4. \end{cases} \quad (4)$$

The four angles θ_i ($i = 1,\ldots,4$), corresponding to four radial positions $r_i = \sin\theta_i/\mathrm{NA}$ (normalized to the optical aperture) were optimized to increase the ratio of the longitudinal and radial components within a long focal region. This is not a strictly defined procedure. Ideally we want to obtain a very narrow beam and also a very long depth of focus (a non-diffracting beam). We want to have high beam quality, high beam homogeneity and also high optical efficiency for conversion of the radially polarized beam to a longitudinally polarized beam. However, it is not possible to optimize all these mentioned quantities simultaneously. In fact, each solution is some compromise between these quantities, and each quantity can be improved by trading off the others. This optimization problem therefore depends on determining the priority of these quantities.

As an example we can suggest the set of angles found from the reasonable optimization of all parameters:

$$\theta_1 = 4.96°,\ \theta_2 = 21.79°,\ \theta_3 = 34.25°,\ \theta_4 = 46.87°. \quad (5)$$

The corresponding positions r_i are given by

$$r_1 = 0.091,\ r_2 = 0.391,\ r_3 = 0.592,\ r_4 = 0.768. \quad (6)$$

The transmission function $T(\theta)$ on the aperture of the focusing lens for this case is shown in Fig. 3a. The electric energy density
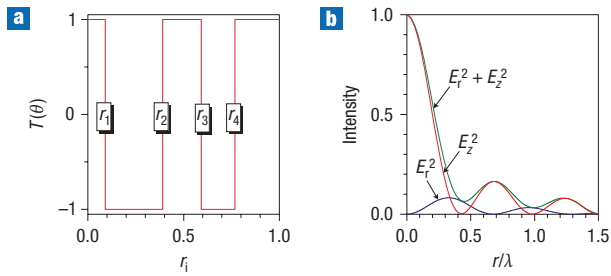
Figure 3 Electric field amplitude transmission function on the aperture and the corresponding electric energy density profile on the focal plane of the NA = 0.95 lens illuminated with a radially polarized Bessel–Gaussian beam after additional phase modulation. **a**, Amplitude transmission function $T(\theta)$. **b**, Electric energy density profile of the radial E_r^2, longitudinal E_z^2 and the total $E_r^2 + E_z^2$ field components.

Figure 4 Contour plots for the electric and magnetic density distributions in the *yz*-plane after additional phase modulation. **a**, Total energy density distribution. **b**, Radial component. **c**, Longitudinal component. **d**, Magnetic energy density.

profiles of the radial component, the longitudinal component, and the total electric field of the beam in the focal cross-section are shown in Fig. 3b. The FWHM of the longitudinal electric field component energy density profile in Fig. 3b is 0.4λ, which is smaller than that shown in Fig. 1a (0.49λ). The FWHM of the total electric energy density spot in Fig. 3b is 0.43λ, so the spot area is $0.15\lambda^2$, which is smaller than that obtained without the binary optical element shown in Fig. 1a (FWHM = 0.68λ). Thus, the beam area is reduced by 58%.

We shall characterize the conversion efficiency of our system as the ratio of the total energy within the focal volume after conversion to its original energy within the focal volume before conversion. Remember that both the energy density and the focal volume are changing. Numerical integration yields a conversion efficiency above 20%. At the same time the beam quality after conversion almost doubles from $\eta = 0.45$ to $\eta = 0.81$.

A contour plot of the total electric energy density image is shown in Fig. 4a and the radial and longitudinal components in Fig. 4b,c. One can see that the total depth of focus is about 4λ, with very uniform axial electric energy density; in other words it is a non-diffracting beam. The modulation function produces a uniform axial electric energy density over a finite range, which is different from that generated by a sinc variation[35]. The radially polarized field given by equations (1) and (2) produces an azimuthally polarized magnetic field with an H_φ component only (similar to the field around a linear conductor carrying current). This field can be found from Maxwell's equations, yielding $H_\varphi = -i(\partial_z E_r - \partial_r E_z)/k$; that is,

$$H_\varphi = 2A \int_0^\alpha \cos^{1/2}\theta \sin(\theta)\ell(\theta)T(\theta)J_1(kr\sin\theta)e^{ikz\cos\theta}\,\mathrm{d}\theta. \quad (7)$$

The density distribution of the magnetic field component H_φ is shown in Fig. 4d. In the focal plane $z = 0$ the field (6) is purely real. Different signs of this field correspond to clockwise and anticlockwise field directions.

DISCUSSION

In principle it is possible to further enhance the longitudinal field by using a lens of higher NA. However with NA > 1, the field attenuates exponentially[36], so the non-diffraction characteristic of the beam is lost. It is also possible to improve the longitudinal field component (and obtain longer depth of focus) by applying
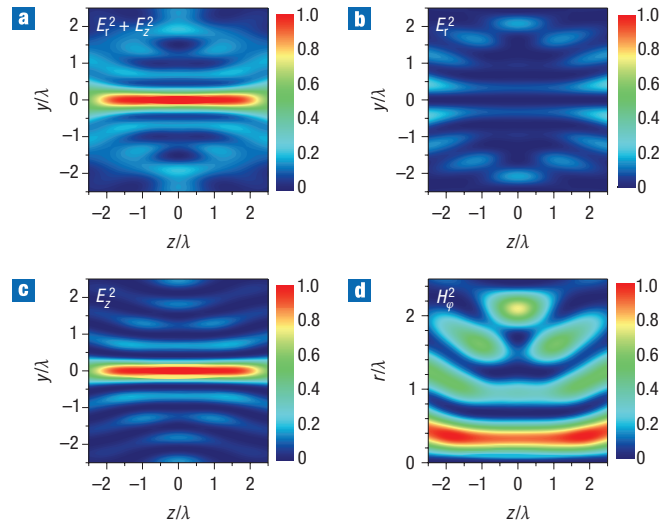
more belts, for example, seven belts instead of the five belts in equation (4). However, the efficiency of optical conversion also drops with an increase in the total number of belts. Thus, the five-belt optical modulation is a compromise between the longitudinal field strength and optical efficiency.

Once again it should be emphasized that a method has been proposed for the formation of uniform, longitudinally polarized light along an axis in free space, where the vanishing of one field component is created by the binary optical element. It is different from the near-field region between two different materials with evanescent or plasmonic waves. The necessary conditions for the field localization in the latter case are fulfilled in a natural way due to exponential electric energy density attenuation. The binary optical element here works like a special polarization filter, which diffracts the radial field component away from beam centre more than the longitudinal field, thus making the beam in the focal region substantially longitudinally polarized. The non-diffraction characteristic of this beam may reduce the diffraction angle of the particles being accelerated[5,9,10,14]; this makes it easier for focusing in second-harmonic generation polarization microscopy[16–18], for the coupling of light to SNOMs (scanning near-field optical microscopes) or nanoplasmonic devices[19,36,37], and enables pure longitudinal field optical coherence tomography[38]. It is different from the non-diffraction linear polarized light suggested in ref. 34, where the super-resolution effect was obtained in the direction perpendicular to the polarization direction, the resolution in the polarization direction being degraded by the cross-polarization effect caused by the binary optical element.

To achieve a better understanding of the mechanism that makes the longitudinal field propagate without divergence, we further investigate the Poynting vector field of the focused radially polarized Bessel–Gaussian beam for arrangement without and with the binary optical element, as shown in Fig. 5a,b, respectively. The time-averaged Poynting vector is determined by

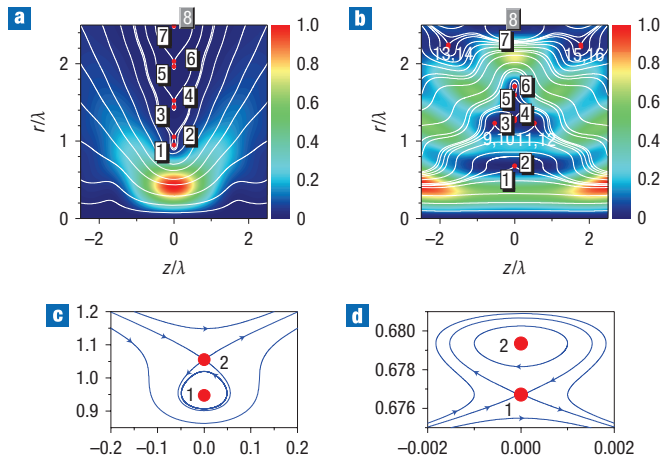$$\langle \mathbf{S} \rangle = \frac{c}{4\pi}\mathrm{Re}(\mathbf{E} \times \mathbf{H}^*), \quad (8)$$

Figure 5 Normalized Poynting vector field (colour density plots) and the energy flow (white field lines). a,c, Original Bessel–Gaussian beam. **b,d,** Field after phase modulation. The singular points are indicated by red circles. **c,d,** Enlarged plots of the energy flow in the vicinity of points 1 and 2: point 1 centre type, point 2 saddle type (**c**); point 1 saddle type, point 2 centre type (**d**). Note that the energy flow direction has changed.

Figure 6 Polarization characteristic of the field in the focal region of the NA = 0.95 lens with a binary optical element. a, Time-averaged polarization of the electric field in the $x-z$ cross-section. **b,c,** Contour plots for the time-domain field distribution at the moment $t = 0$: longitudinal field component E_z (**b**) and radial field component E_r (**c**).

where the asterisk denotes the operation of complex conjugation. This field is axially symmetric because of the condition $S_\varphi = 0$. Thus, the field lines of the Poynting vector follow the equation $\mathrm{d}r/\mathrm{d}z = S_r/S_z$. The Poynting vector field contains circular singular lines, which for the radially polarized Bessel–Gaussian beam are distributed in the focal plane $z = 0$. A cross-section of these lines by the yz-plane corresponds to the singular points 1 to 8 in Fig. 5a. The singularities consist of four couples of saddle- and centre-type points, which are shown with larger scale in Fig. 5c (for the couple comprising points 1 and 2). One can see a similar behaviour for the couple formed of singular points 3 and 4, and so on. Centre-type points 1, 3, 5 and 7 are situated inside the loop of separatrix. They correspond to points with $H_\varphi = 0$. Saddle-type points 2, 4, 6 and 8 correspond to points with $E_r = 0$.

The Poynting vector field for the longitudinally polarized beam in Fig. 5b contains eight further singular points when compared with Fig. 5a. Couples of these points (9, 10, and so on) are distributed at some distances $z \neq 0$ from the focal plane. Comparing Fig. 5a and Fig. 5b one can clearly see that the time-averaged Poynting vector field near the axis becomes more homogeneous after phase modulation. It is of purely geometrical origin. Phase modulation permits the inversion of the positions of the saddle and centre points (1 and 2) in Fig. 5c and Fig. 5d. The field is less homogeneous from the side of the separatrix loop (because the loop contains infinite vertical derivations). Thus, the field near the axis in Fig. 5d is more homogeneous than that in Fig. 5c. In a similar way the inhomogeneity that is produced by the loop around point 3 (situated below saddle point 4), is compensated due to the homogenizing action of inversely situated loops of the separatrices around the near points 6, 10 and 12 (situated above the corresponding saddle points).

Similar singularities of the Poynting vector for a focused beam are well known[6,39]. They also arise for example, during scattering of light by nanoparticles and nanowires near plasmon resonance frequencies[37,40,41]. It is important here that the Poynting vector field near the axis is almost uniform along the propagation direction (see the almost straight lines in Fig. 5b at $r/\lambda < 0.3$).
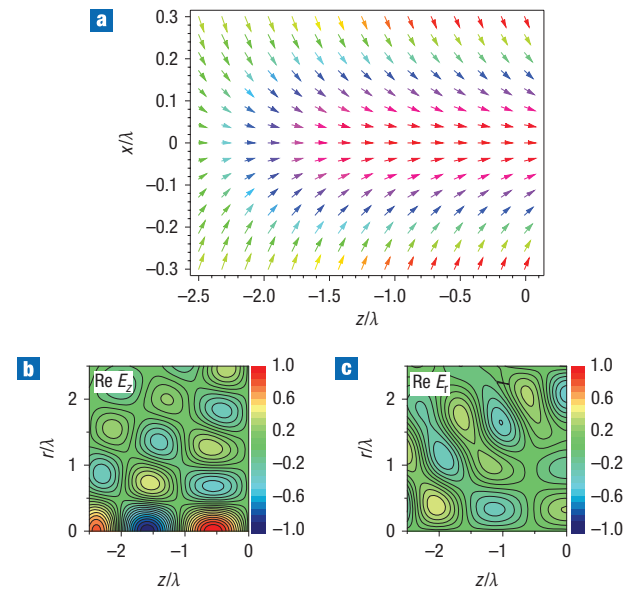
To show the field polarization we plot in Fig. 6a the distribution of the averaged electric field, where the radial component is understood as modulus $|E_r| = [E_r(r, z)E_r^\star(r, z)]^{1/2}$ and the longitudinal component as the modulus $|E_z| = [E_z(r, z)E_z^\star(r, z)]^{1/2}$. The direction of this vector was selected with positive sign along the z-axis. One can see that in the periphery of the beam incoming radiation there is a noticeable contribution of radially polarized light, but in the near-axial region, where the basic electric energy density is localized (see Fig. 4a), the field has practically homogeneous longitudinal polarization. In contrast to the usual situation in which a beam diverges after the focal plane and attenuates exponentially[42–44], our longitudinally polarized beam looks like a needle as shown in Fig. 4a.

The dynamic distribution of the field Re $E(r, z, t)$ is quite complicated; it is shown in Fig. 6b,c for the moment of time $t = 0$. Once again, we can see from the figure that the field is essentially longitudinally polarized near the axis. Various peculiarities, such as dislocations of the wavefront and optical vortices, exist for this field. Although these peculiarities do not influence our basic effect (longitudinally polarized light needle), they may be of interest in other applications[45].

In conclusion, we have proposed the generation of a longitudinally polarized beam by focusing a radially polarized beam using a binary optical element and a lens. This binary optical element works like a special polarization filter, which diffracts the radial field away from the centre of the beam more than the longitudinal field, thus making the beam in the focal region substantially longitudinally polarized. This beam propagates without divergence for over 4λ (a non-diffracting beam). It is also highly localized in the transverse direction with FWHM $= 0.43\lambda$ (subdiffraction beam). The suggested method achieves the required combination of conversion efficiency, uniformity and field localization.

Note that recent methods for creation of a needle of linearly polarized light have been suggested both theoretically[34,46] and

experimentally[38,47,48]. Now we can see that the formation of a needle of longitudinally polarized light is also possible with the help of phase modulation.

References

1. Sheppard, C. J. R. & Saghafi, S. Transverse-electric and transverse-magnetic beam modes beyond the paraxial approximation. *Opt. Lett.* **24**, 1543–1545 (1999).
2. Dorn, R., Quabis, S. & Leuchs, G. Sharper focus for a radially polarized light beam. *Phys. Rev. Lett.* **91**, 233901 (2003).
3. Kozawa, Y., Yonezawa, K. & Sato, S. Radially polarized laser beam from a Nd:YAG laser cavity with a c-cut YVO$_4$ crystal. *Appl. Phys. B* **88**, 43–46 (2007).
4. Richard, B. & Wolf, E. Electromagnetic diffraction in optical systems. II. Structure of the image field in an aplanatic system. *Proc. Roy. Soc. A* **253**, 358–379 (1959).
5. Cicchitelli, L., Hora, H. & Postle, R. Longitudinal field components for laser beams in vacuum. *Phys. Rev. A* **41**, 3727–3732 (1990).
6. Sheppard, C. J. R. Electromagnetic field in the focal region of wide-angular annular lens and mirror systems. *Microw. Opt. Acoust.* **2**, 163–166 (1978).
7. Ganic, D., Gan, X. & Gu, M. Focusing of doughnut laser beams by a high numerical-aperture objective in free space. *Opt. Express* **11**, 2747–2752 (2003).
8. Lee, K. G. *et al.* Vector field microscopic imaging of light. *Nature Photon.* **1**, 53–56 (2006).
9. Fontana, J. R. & Pantell, R. H. A high-energy, laser accelerator for electrons using the inverse Cherenkov effect. *J. Appl. Phys.* **54**, 4285–4288 (1983).
10. Romea, R. D. & Kimura, W. D. Modelling of inverse Čerenkov laser acceleration with axicon laser-beam focusing. *Phys. Rev. D* **42**, 1807–1818 (1990).
11. Bouchal, Z. & Olivik, M. Non-diffractive vector Bessel beams. *J. Modern Opt.* **42**, 1555–1566 (1995).
12. Sheppard, C. J. R. & Török, P. Electromagnetic field in the focal region of an electric dipole wave. *Optik* **104**, 175–177 (1997).
13. Sun, C.-C. & Liu, C.-K. Ultrasmall focusing spot with a long depth of focus based on polarization and phase modulation. *Opt. Lett.* **28**, 99–101 (2003).
14. Rosenzweig, J., Murokh, A. & Pellegrini, C. A proposed dielectric-loaded resonant laser accelerator. *Phys. Rev. Lett.* **74**, 2467–2470 (1995).
15. Novotny, L. *et al.* Longitudinal field modes probed by single molecules. *Phys. Rev. Lett.* **86**, 5251–5254 (2001).
16. Bouhelier, A. *et al.* Near-field second-harmonic generation induced by local field enhancement. *Phys. Rev. Lett.* **90**, 013903 (2003).
17. Biss, D. P. & Brown, T. G. Polarization-vortex-driven second-harmonic generation. *Opt. Lett.* **28**, 923–925 (2003).
18. Yew, E. Y. S. & Sheppard, C. J. R. Second harmonic generation polarization microscopy with tightly focused linearly and radially polarized beams. *Opt. Commun.* **275**, 453–457 (2007).
19. Hayazawa, N., Saito, Y. & Kawata, S. Detection and characterization of longitudinal field for tip-enhanced Raman spectroscopy. *Appl. Phys. Lett.* **85**, 6239–6241 (2004).
20. Huse, N., Schonle, A. & Hell, S. W. Z-polarized confocal microscopy. *J. Biomed. Opt.* **6**, 480–484 (2001).
21. Xiao, M. Theoretical treatment for scattering scanning near-field optical microscopy. *J. Opt. Soc. Am. A* **14**, 2977–2984 (1997).
22. Sheppard, C. J. R. & Choudhury, A. Annular pupils, radial polarization and superresolution. *Appl. Opt.* **43**, 4322–4327 (2004).
23. Machavariani, G. *et al.* Efficient extracavity generation of radially and azimuthally polarized beams. *Opt. Lett.* **32**, 1468–1470 (2007).
24. Sheppard, C. J. R. High-aperture beams. *J. Opt. Soc. Am. A* **18**, 1579–1587 (2001).
25. Dorn, R., Quabis, S. & Leuchs, G. The focus of light—linear polarization breaks the rotational symmetry of the focal spot. *J. Modern Opt.* **50**, 1917–1926 (2003).
26. Meyer, M., Romano, V. & Feurer, T. Material processing with pulsed radially and azimuthally polarized laser radiation. *Appl. Phys. A* **86**, 329–334 (2007).
27. Sheppard, C. J. R. & Wilson, T. Gaussian-beam theory of lenses with annular aperture. *Microw. Opt. Acoust.* **2**, 105–112 (1978).
28. Youngworth, K. S. & Brown, T. G. Focusing of high numerical aperture cylindrical-vector beams. *Opt. Express* **7**, 77–87 (2000).
29. Durnin, J., Miceli, J. J. Jr, & Eberly, J. H. Diffraction-free beams. *Phys. Rev. Lett.* **58**, 1499–1501 (1987).
30. Campos, J. *et al.* Axially invariant pupil filters. *J. Modern Opt.* **47**, 57–68 (2000).
31. Li, Y., Lee, H. & Wolf, E. New generalised Bessel–Gaussian beams. *J. Opt. Soc. Am. A* **21**, 640–646 (2004).
32. Visser, T. D. & Foley, J. T. On the wavefront spacing of focused, radially polarized beams. *J. Opt. Soc. Am. A* **22**, 2527–2531 (2005).
33. Sheppard, C. J. R. Binary optics and confocal imaging. *Opt. Lett.* **24**, 505–506 (1999).
34. Wang, H. *et al.* Subwavelength and super-resolution non-diffraction beam. *Appl. Phys. Lett.* **89**, 171102 (2006).
35. Sheppard, C. J. R. Synthesis of filters for specified axial properties. *J. Modern Opt.* **43**, 525–536 (1996).
36. Zhan, Q. Evanescent Bessel beam generation via surface plasmon resonance excitation by a radially polarized beam. *Opt. Lett.* **31**, 1726–1728 (2006).
37. Luk'yanchuk, B. S. & Ternovsky, V. Light scattering by a thin wire with a surface-plasmon resonance: Bifurcations of the Poynting vector field. *Phys. Rev. B* **73**, 235432 (2006).
38. Liu, L. *et al.* Binary-phase spatial filter for real-time swept-source optical coherence microscopy. *Opt. Lett.* **32**, 2375–2377 (2007).
39. Boivin, A., Dow, J. & Wolf, E. Energy flow in the neighbourhood of the focus of a coherent beam. *J. Opt. Soc. Am.* **57**, 1171–1175 (1967).
40. Wang, Z. B. *et al.* Energy flow around a small particle investigated by classical Mie theory. *Phys. Rev. B* **70**, 035418 (2004).
41. Tribelsky, M. I. & Luk'yanchuk, B. S. Anomalous light scattering by small particles. *Phys. Rev. Lett.* **97**, 263902 (2006).
42. Lezec, H. J. *et al.* Beaming light from a subwavelength aperture. *Science* **297**, 820–822 (2002).
43. Kalosha, V. P. & Golub, I. Toward the subdiffraction focusing limit of optical super-resolution. *Opt. Lett.* **32**, 3540–3542 (2007).
44. Hao, B. & Leger, J. Experimental measurement of longitudinal component in the vicinity of focused radially polarized beam. *Opt. Express* **15**, 3550–3556 (2007).
45. Vasnetsov, M. & Staliunas, K. *Optical Vortices* (Nova Science, Commack, 1999).
46. Wang, H. & Gan, F. High focal depth with a pure-phase apodizer. *Appl. Opt.* **40**, 5658–5662 (2001).
47. Wang, H. & Gan, F. Phase-shifting apodizers for increasing focal depth. *Appl. Opt.* **41**, 5263–5266 (2002).
48. Botcherby, E. J., Juškaitis, R. & Wilson, T. Scanning two photon fluorescence microscopy with extended depth of field. *Opt. Commun.* **268**, 253–260 (2006).